Refinements to the method of epicentral location based on surface waves from ambient seismic noise: introducing Love waves

Anatoli L. Levshin,[1] Mikhail P. Barmin,[1] Morgan P. Moschetti,[2] Carlos Mendoza[3] and Michael H. Ritzwoller[1]

[1]*Department of Physics, University of Colorado at Boulder, Boulder, CO 80309, USA. E-mail: levshin@colorado.edu*
[2]*Geological Hazards Science Center, U.S. Geological Survey, Golden, CO 80401, USA*
[3]*Centro de Geociencias, Universidad Nacional Autonoma de Mexico, Queretaro, 76230, Mexico*

SUMMARY

The purpose of this study is to develop and test a modification to a previous method of regional seismic event location based on Empirical Green's Functions (EGFs) produced from ambient seismic noise. Elastic EGFs between pairs of seismic stations are determined by cross-correlating long ambient noise time-series recorded at the two stations. The EGFs principally contain Rayleigh- and Love-wave energy on the vertical and transverse components, respectively, and we utilize these signals between about 5 and 12 s period. The previous method, based exclusively on Rayleigh waves, may yield biased epicentral locations for certain event types with hypocentral depths between 2 and 5 km. Here we present theoretical arguments that show how Love waves can be introduced to reduce or potentially eliminate the bias. We also present applications of Rayleigh- and Love-wave EGFs to locate 10 reference events in the western United States. The separate Rayleigh and Love epicentral locations and the joint locations using a combination of the two waves agree to within 1 km distance, on average, but confidence ellipses are smallest when both types of waves are used.

Key words: Earthquake source observations; Surface waves and free oscillations; Theoretical seismology.

GJI Seismology

1 INTRODUCTION

In a previous study, Barmin *et al.* (2011), referred to hereafter as Paper I, presented a new approach to the epicentral location of shallow seismic events based on the use of the Empirical Green's Functions (EGFs) obtained from ambient seismic noise. The vertical component of the ambient noise in the period range from 7 to 15 s, which is dominated by the fundamental Rayleigh wave, was used to compute the EGFs. It was demonstrated that this approach has several features that make it a useful addition to existing location methods. First, the method is based on surface waves, which are usually not applied in most location algorithms. Second, it does not require knowledge of the Earth structure and is, therefore, unbiased by uncertainties in the knowledge of structure near the epicentre. Third, it works well for weak seismic events even if the detection of body wave phases is problematic. Fourth, the EGFs computed during a temporary deployment of a base network [such as the USArray Transportable Array (TA) or PASSCAL deployments] may be applied to events that occur earlier or later using permanent remote stations even if the temporary stations are absent. However, the method has several evident limitations. In particular, it is based on the assumption that the event source mechanism and depth are unknown and does not attempt to estimate them. Time-shifts in the surface waves caused by the source mechanism, therefore, can bias the epicentral location. Paper I shows that this degradation is worst for source depths between about 2 and 5 km if the source mechanism is different from pure strike-slip, thrust or normal faulting. In this case, the method described in Paper I will deliver a biased estimate of the epicentral location.

This paper addresses this limitation by introducing Love waves into the location method. Love waves possess different sensitivity to the source mechanism than Rayleigh waves and, in fact, Love-wave source phase times are quantitatively less sensitive to the source mechanism (Levshin *et al.* 1999). Love waves are, however, in many cases more difficult to observe than Rayleigh waves due to higher noise levels on horizontal components. Epicentral estimates based on Love waves, therefore, have a larger variance than those based on Rayleigh waves, on average. Thus, the joint application of Rayleigh and Love waves to estimate epicentral locations may be preferable to the locations based on either wave type alone, as it strikes a balance between bias and variance.

The outline of the paper is as follows. First, we discuss the modification of the location algorithm to include Love waves. Second,

we discuss the theoretical advantage of jointly applying Rayleigh and Love waves in the location procedure. Finally, we describe the application of the location algorithm to several well-located events in the western United States (California, Utah and Nevada).

2 MODIFICATIONS TO THE LOCATION ALGORITHM

The algorithm defined in Paper I is described in that paper in great detail. A general description of that location method is presented here as well as its modifications and the extension to include Love waves. A seismic event occurs near a set of seismic stations, called the 'base stations'. It is observed at a disjoint set of stations that lie significantly farther from the event, called the 'remote stations'. These time-series are called the 'event records'. In addition, cross-correlations between long time records of ambient noise exist between the base and remote stations, which provide what are called "Empirical Green's functions" (EGFs). Low amplitude event records and EGFs are discarded if their signal-to-noise ratio (SNR) is below 10, where SNR is defined by Bensen *et al.* (2007). Frequency–time analysis (FTAN, e.g. Levshin *et al.* 1972; Levshin & Ritzwoller 2001; Bensen *et al.* 2007) is performed on the event records and the EGFs, producing for each remote station an FTAN diagram for the event and for each interstation pair (base-to-remote) an FTAN diagram for the EGF. The location procedure considers a set of hypothetical event epicentral locations and one is chosen that brings the FTAN diagrams from the event into optimal agreement with the FTAN diagrams for the EGFs. Technically, this comparison is performed by cross-correlation in time between the FTAN diagrams (Levshin *et al.* 1989; Bensen *et al.* 2007).

Examples of several event records and EGFs observed in the western United States are shown in Fig. 1. The event records follow one of the aftershocks of the Wells earthquake in Nevada in 2008 (Mendoza & Hartzell 2009) that occurred on April 22, with a magnitude of 4.4, and an epicentre located at a distance of about 23 km from TA station M12A (aftershock #6, Table 1). The map in Fig. 1(a) locates the epicentre and selected remote TA stations north and south of station M12A. Rayleigh and Love waves are distinctly seen in the event record in Fig. 1(b) at station H12A at an epicentral distance of about 370 km. Record sections of Z-Z and T-T EGFs for the base station M12A and selected remote stations are shown in Figs 1(c) and (d). The symmetric component of the EGFs is plotted and used here in every instance. Record sections of vertical and transverse components of the observed event seismograms are similarly presented in Figs 1(e) and (f). There is a general similarity of SNR as well as the arrival times of the EGFs and event records, but the frequency contents of the two types of waves differ with the EGFs being enriched at somewhat longer periods than the event records. In addition, examples of FTAN diagrams for Rayleigh- and Love-wave event records also following Wells aftershock #6 and EGFs are shown in Fig. 2. FTAN diagrams for the event records observed at remote station K16A, about 321 km northeast of the inferred epicentral location, are in Figs 2(c) and (d). The FTAN diagrams of the EGFs between stations K16A and M12A (near the epicentre) are shown in Figs 2(a) and (b). Rayleigh and Love waves are shown to arrive at clearly different times with the Love waves arriving earlier, from which we conclude that the waves observed on the transverse component are, in fact, Love waves.

The algorithm of Paper I progresses by searching a grid of hypothetical event locations. For each hypothetical event location, all of the EGFs are effectively shifted to the hypothetical location by changing the interstation distance under the assumption that the group velocity measured at the remote station remains unchanged when shifting from the base station location to the epicentral location. This spatial shift of the base station is, therefore, converted to a time-shift that stretches or compresses the time axis on the FTAN diagram for each EGF. Then, for each hypothetical event location and all remote stations, the FTAN diagram for each EGF is cross-correlated with the FTAN diagram of the event record observed at the appropriate remote station. This results in a set of cross-correlations each of which can be summarized by an offset time. The mean of the offset times over all remote stations defines the corrected origin time. The rms of the offset times computed relative to the corrected origin time over all remote stations defines the misfit for that hypothetical event location. The algorithm searches systematically over a spatial grid and maps rms misfit, from which an epicentral location is determined as well as an error ellipse (Flinn 1965; Jordan & Swerdrup 1981).

The reliability of the procedure of Paper I, however, is degraded by a number of vagaries of FTAN diagrams as well as the existence of several *ad hoc* parameters that are set in the algorithm. FTAN diagrams may have spectral holes as well as coda that are quite variable, which makes them difficult to compare directly. For example, for an earthquake at a given depth the event record may have a spectral hole between 10 and 15 s period, say, which is not found in the EGFs. These issues render FTAN diagrams non-ideal as a basis for operational application. In this paper, in addition to introducing Love waves, we have modified the method to improve its stability by removing its dependence on comparing FTAN diagrams. The modification also simplifies and speeds up the algorithm substantially.

The modification to this algorithm that we apply here is to replace the FTAN diagrams with group velocity curves computed from the event record and the EGFs, respectively. Thus, group times determined from the FTAN diagrams are compared rather than comparing the offset times from the cross-correlations of the FTAN diagrams. This simplifies the algorithm considerably and also stabilizes it because the group times observed on an FTAN diagram are more stable than the details of the FTAN diagram itself. The FTAN algorithm that we apply has been tuned through extensive use to return group time measurements only in the band in which the measurements are reliable. When comparing a particular EGF to an event record, we compute the rms difference between the observed group times only in the period band in which both measured curves are reliable. This band as wide is typically about 6–12 s period.

In practice, the rms misfit is computed between the group times observed on the event records and those observed on the EGFs between each base-to-remote station-pair where each base station has been shifted theoretically to the hypothetical event location (θ,ϕ), where θ and ϕ are latitude and longitude, respectively. This theoretical shift of the base station is accomplished similarly to the method of Paper I by modifying the observed group time (determined now from the observed group velocity) of the EGF by changing the interstation distance to the epicentral distance. Let $u_j(\omega_k)$ and $v_j(\omega_k)$ be the event group times at discrete frequency ω_k for Rayleigh and Love waves, respectively, observed at remote station j. An initial event time t_0 must be assumed for the group times of the event to be determined. There are also a set of group times measured for each of the EGFs between the base station i shifted to hypothetical epicentral location (θ,ϕ) to the remote station j, which is referred to as $\hat{u}_{ij}(\omega_k, \theta, \varphi)$. We separately compute the misfit between the event and EGF group times for the Rayleigh waves and the Love
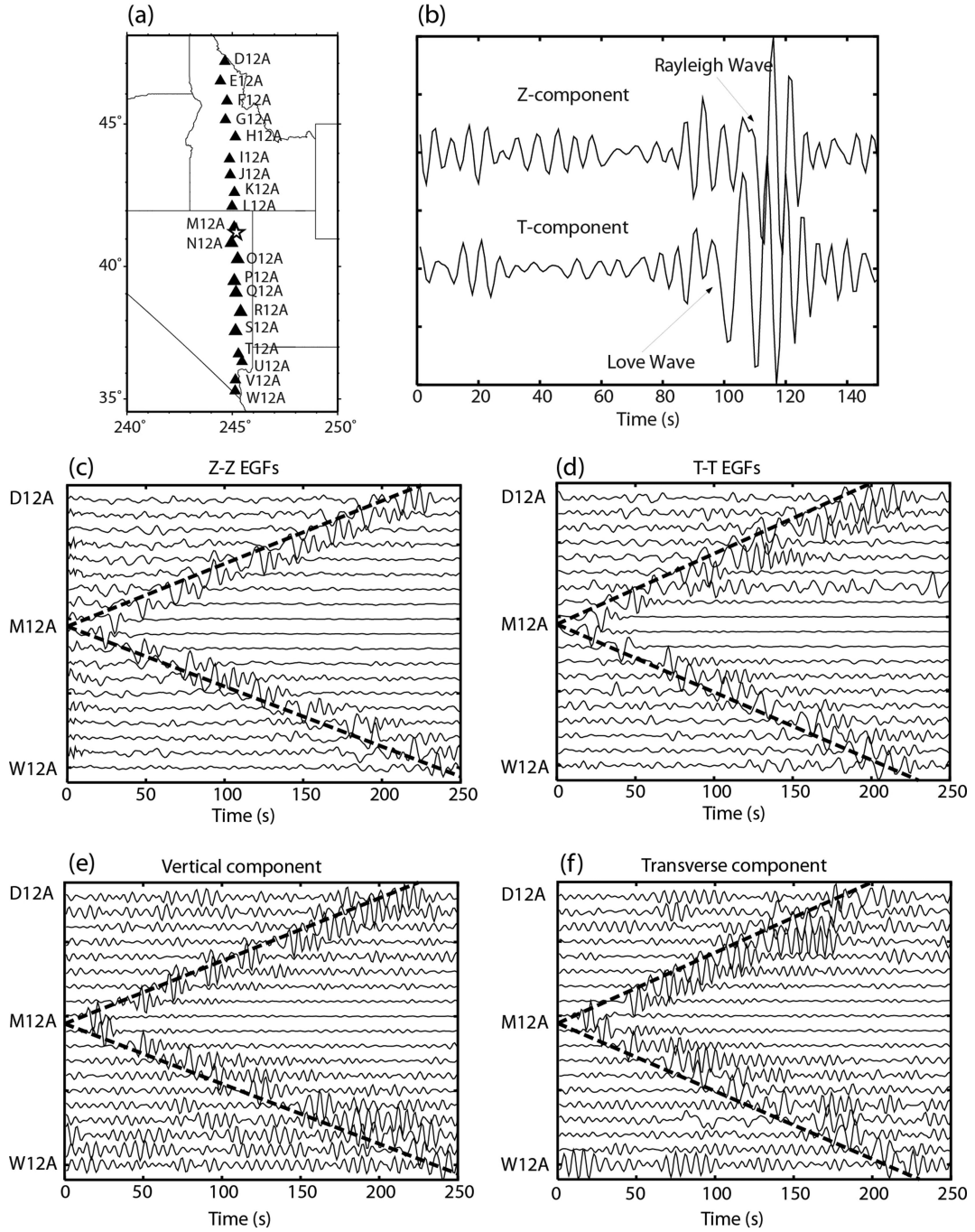
Figure 1. (a) Map of stations (triangles) selected near the meridian passing through the epicentre (star) of aftershock #6 on 2008 April 22 of the Wells earthquake in Nevada. (b) Vertical and transverse component seismograms following the aftershock observed at TA station H12A located about 370 km north of the epicentre identifying Rayleigh and Love waves. (c) Symmetric component Z-Z (Rayleigh wave) interstation empirical Green's functions (EGFs) for the base station M12A and selected remote stations. (d) Same as (c) but for symmetric component T-T (Love wave) interstation EGFs. (e) Vertical component event records observed at the remote stations following the aftershock. (f) The same as (e) but for transverse components. Straight lines in (c)–(f) indicate predicted times of arrivals for Rayleigh and Love waves with group velocities of 2.95 and 3.3 km s^{-1}, respectively.

waves, summing over remote stations, base stations and discrete frequencies. We refer to these rms misfits as F_R and F_L:

$$F_R^2(\theta, \phi) = N^{-1} \sum_{k=1}^{K} \sum_{j=1}^{J} \sum_{i=1}^{I} \left(u_j(\omega_k) - \hat{u}_{ij}(\omega_k, \theta, \phi) \right)^2,$$

$$F_L^2(\theta, \phi) = M^{-1} \sum_{k=1}^{K} \sum_{j=1}^{J} \sum_{i=1}^{I} \left(v_j(\omega_k) - \hat{v}_{ij}(\omega_k, \theta, \phi) \right)^2,$$

where i indexes the sum over the base stations, j represents the sum over the remote stations, k is the discrete frequency index, and I, J, K are the numbers of base stations, remote stations and discrete frequencies in the band of analysis, respectively. In the ideal case in which all the base stations and remote stations are used and all measurements extend over the entire frequency band of analysis, the number of discrete measurable quantities $M = N = IJK$. In practice, however, both the event records and EGFs are selected

Table 1. Reference event parameters.

Event	Date (y/m/d)	Origin time	Latitude (N)	Longitude (W)	Depth (km)	*M*	Reference
Earthquake, CA	2005/04/16	19:18:13.0	35.027	119.178	10.8	4.9	CT
Mine collapse, UT	2007/08/06	08:48:39.9	39.467	111.225	0.5	3.9	P
Earthquake, UT	2007/08/18	13:16:30.5	38.070	113.323	9.0	3.6	UUSS
Wells Event, NV	2008/02/21	14:16:02.7	41.160	114.877	10.0	6.3	UNR/H
Aftershock#1	2008/02/21	23:57:51.0	41.151	114.931	10.0	4.6	UNR/H
Aftershock#2	2008/02/22	01:50:05.2	41.142	114.923	10.0	3.9	UNR/H
Aftershock#3	2008/02/22	23:27:45.2	41.104	114.917	10.0	4.2	UNR/H
Aftershock#4	2008/02/28	15:10:37.8	41.157	114.929	10.0	3.9	UNR/H
Aftershock#5	2008/04/01	13:16:17.3	41.228	114.840	7.6	4.2	UNR/H
Aftershock#6	2008/04/22	20:40:09.4	41.221	114.806	7.7	4.4	UNR/H

Note: Information comes from the following sources: CT refers to the Caltech Seismological Laboratory; P refers to Pechmann *et al.* (2007); UUSS stands for Bulletins of the University of Utah Seismograph Stations; UNR refers to Seismological Laboratory of the University of Nevada Reno for locations and origin times, and source depths and magnitudes come from reference H, Herrmann *et al.* (2011).
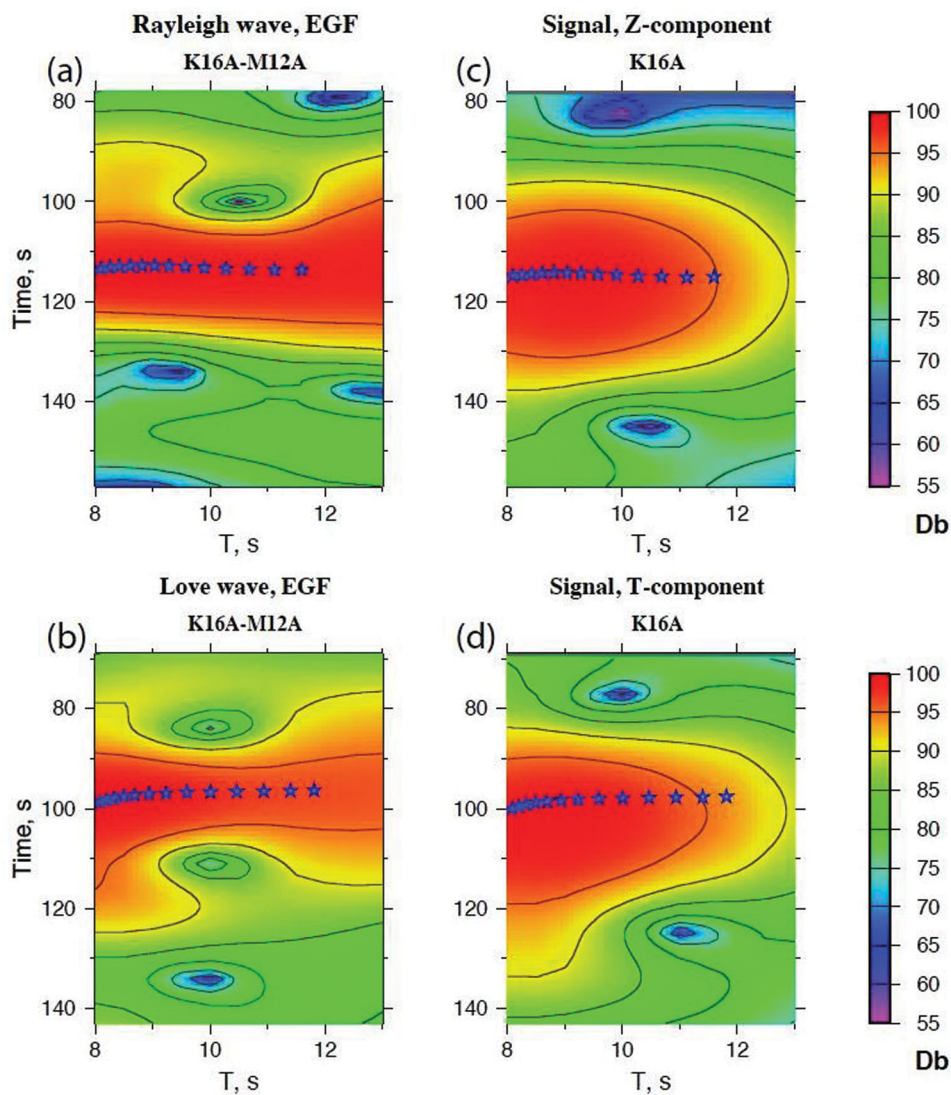

Figure 2. (a, b) FTAN diagrams for Rayleigh- and Love-wave symmetric component EGFs for a pair of TA stations (K16A-M12A) compared with (c) and (d) the FTAN diagrams of the corresponding event records from the earthquake in Fig. 1 observed at station K16A (location shown in Fig. 1a). Blue stars are group times determined by FTAN.
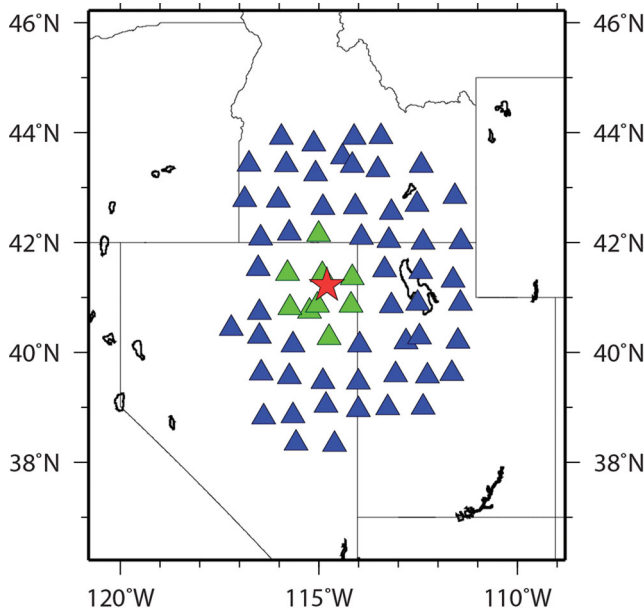
Figure 3. The network of base (green triangles) and remote (blue triangles) stations used to locate the large Wells earthquake that occurred in northern Nevada (red star) on 2008 February 21 and for six of its aftershocks (#1–#6) that occurred from 2008 late February to late April.

based on SNR and individual measurements often extend over only a subband; thus, the number of measurables will differ between Rayleigh and Love waves ($M \neq N$) and both will be less than the product IJK. The units of F_R and F_L are seconds. These misfit functionals are spatial surfaces because a misfit value exists for each point on the spatial grid of hypothetical epicentral locations.

For each hypothetical event location (θ, ϕ) on each misfit surface, the assumed initial event time must be corrected based on the average of the unsquared misfit:

$$\Delta t_R(\theta, \phi) = N^{-1} \sum_{k=1}^{K} \sum_{j=1}^{J} \sum_{i=1}^{I} \left(u_j(\omega_k) - \hat{u}_{ij}(\omega_k, \theta, \phi) \right),$$

$$\Delta t_L(\theta, \phi) = M^{-1} \sum_{k=1}^{K} \sum_{j=1}^{J} \sum_{i=1}^{I} \left(v_j(\omega_k) - \hat{v}_{ij}(\omega_k, \theta, \phi) \right).$$

Example maps of the misfit functionals $F_R(\theta, \phi)$ and $F_L(\theta, \phi)$ as well as confidence ellipses for the Wells aftershock #6 on 2008 April 22 for the base and remote stations shown in Fig. 3 are presented in Figs 4(a) and (b), respectively. As for most earthquakes, the Love-wave error ellipse is larger than the Rayleigh-wave ellipse because the SNR for the Love waves is lower than for Rayleigh waves and, everything else being equal, the Love-wave misfit is higher. The accuracy of the reference location is not known, thus the difference between the estimated location and the reference location is not used as a quality criterion. The Rayleigh-wave location is very similar to the location determined with the previous algorithm presented in Paper I, but the computation time has been reduced by a factor of about 20.

In addition, we compute the joint Rayleigh–Love misfit functional, $F_{RL}(\theta, \phi)$:

$$F_{RL}(\theta, \phi) = \lambda_R F_R(\theta, \phi) + \lambda_L F_L(\theta, \phi), \tag{1}$$

in which we introduce weights λ_R and λ_L, such that $\lambda_R + \lambda_L = 1$. In the joint functional, Rayleigh- and Love-wave misfits can be weighted equally ($\lambda_R = \lambda_L = 0.5$) or differently depending

on the level of misfit, the average SNR, some other indication of measurement quality or discrepancy from a prior estimate of the location. The correction to the initial event time is also found in the joint location scheme for each point on the grid: $\Delta t_{RL} = \lambda_R \Delta t_R + \lambda_L \Delta t_L$. Weighting schemes are discussed further later, although the choice of an optimal weighting scheme is not a major focus here. The joint location algorithm seeks to find the epicentral location that minimizes F_{RL} modulo a given weighting scheme. Examples of joint misfit functionals $F_{RL}(\theta, \phi)$ are shown in Figs 4(c) and (d) in which different weighting schemes have been used. In Fig. 4(c) the Rayleigh and Love waves are given equal weight but in Fig. 4(d) the two contributions are weighted inversely by the minimum misfit found for each wave type, where the weight parameters are $\lambda_R = 0.59$ and $\lambda_L = 0.41$ for this event. Differential weighting is discussed further later.

3 THE ADVANTAGE OF USING BOTH RAYLEIGH AND LOVE WAVES FOR EPICENTRAL LOCATION

Following Aki & Richards (1980) and Levshin *et al.* (1989), the azimuthal dependence of the displacement spectrum for a Love wave at a given frequency excited by a point double-couple source at a depth h in a laterally homogeneous Earth is given by the complex function E:

$$\begin{aligned} E(\varphi, \omega, h) &= ik(\omega)V_3(h, \omega)\left[\left(M_{xx} - M_{yy}\right) \sin\varphi \cos\varphi \right. \\ &\quad \left. + M_{xy} \cos 2\varphi \right] + V_3'(h, \omega)\left[M_{yz} \cos\varphi - M_{xz} \sin\varphi \right], \end{aligned} \tag{2}$$

where $k(\omega)$ is the wavenumber which depends on frequency ω, M_{ij} is a moment tensor component, V_3 is the Love-wave eigenfunction, φ is azimuth taken clockwise from north and $V_3'(h, \omega) = \left(\frac{dV_3}{dz}(z, \omega) \right)\big|_{z=h}$.

The Rayleigh wave expression for the displacement spectrum similar to eq. (1) is

$$\begin{aligned} E(\varphi, \omega, h) &= V_2'(h, \omega)M_{zz} + k(\omega)V_1(h, \omega)\left[\left(M_{xx} \cos^2\varphi \right.\right. \\ &\quad \left. + 2M_{xy} \cos\varphi \sin\varphi - M_{yy} \sin^2\varphi\right) \right] \\ &\quad + i\left[V_1'(h, \omega) - k(\omega)V_2(h, \omega) \right]\left[M_{xz} \cos\varphi + M_{yz} \sin\varphi \right], \end{aligned} \tag{3}$$

where V_1 and V_2 are the horizontal and vertical components of the Rayleigh vectoral eigenfunction and $V_1'(h, \omega)$ and $V_2'(h, \omega)$ are defined similar to $V_3'(h, \omega)$. The modulus $|E|$ of the complex function E represents the source amplitude radiation pattern and the argument $\gamma = \arg(E)$ represents the source phase time delay. Both $|E|$ and γ are real functions of frequency ω, azimuth φ and source depth h. The source phase time delay produces phase shifts in the event seismograms, but our location method is not sensitive to source phase time delays but rather to source group time delays, δt_U, which are the frequency derivative of the source phase time delays (Levshin *et al.* 1999). The real part of eq. (2) and the imaginary part of eq. (3) are proportional to the tangential component of stress and equal zero for a seismic event at the surface $h = 0$. This means that γ is independent of ω for a surface event. Thus, source group time delays are zero for a surface source but for events below the surface will vary depending on azimuth. The source group time delay may be expressed explicitly as

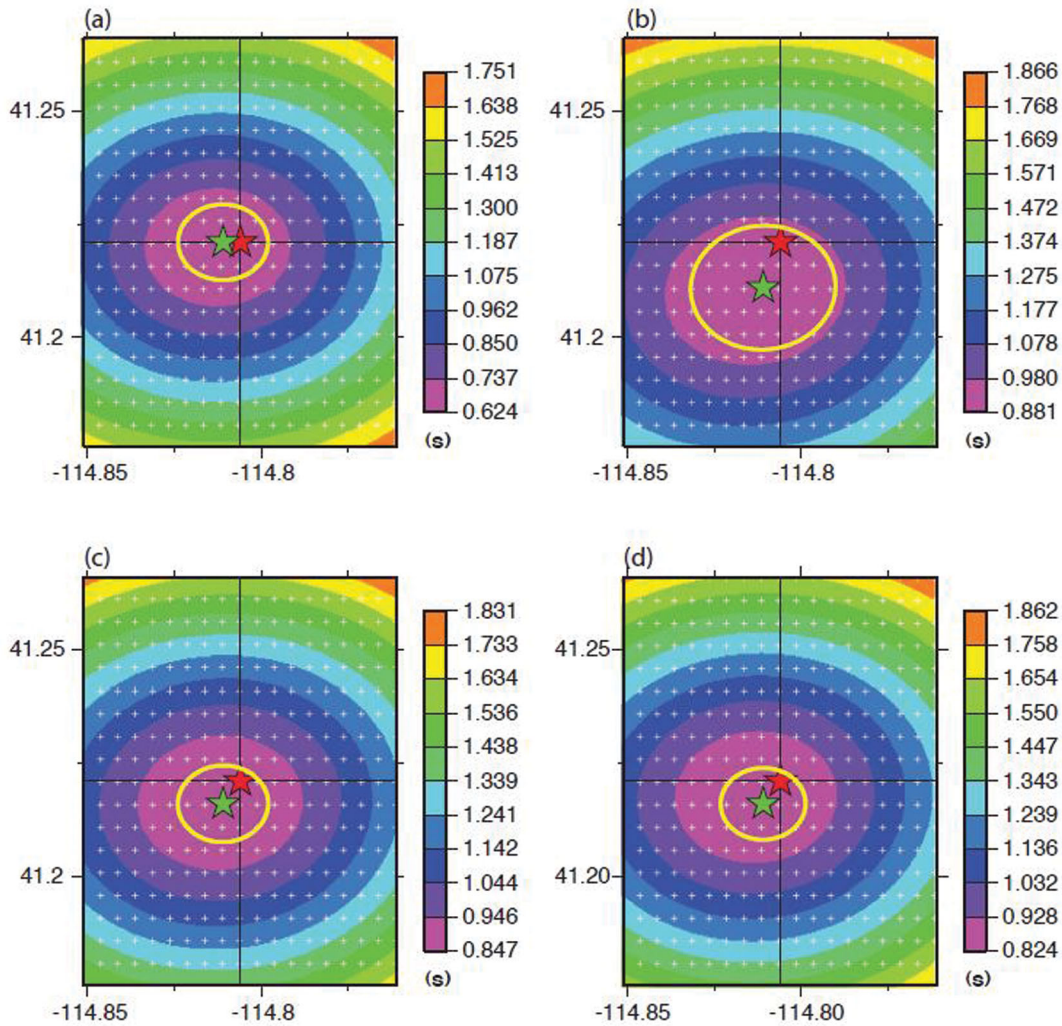$$\delta t_U = \frac{\partial \gamma}{\partial \omega} = \mathrm{Im}\frac{E_\omega' E^*}{|E|^2}. \tag{4}$$

Figure 4. (a) Rayleigh-wave misfit surface $F_R(\theta, \phi)$, in seconds, for aftershock #6 of the Wells earthquake that occurred on 2008 April 22. (b) Love-wave misfit surface $F_L(\theta, \phi)$ for the same aftershock. (c) Joint misfit surface for the same aftershock where Rayleigh and Love waves have been weighted identically ($\lambda_R = \lambda_L = 0.5$). (d) Joint misfit surface for the same aftershock where Rayleigh and Love waves have been weighted inversely by minimum misfit ($\lambda_R = 0.59$, $\lambda_L = 0.41$). The grid spacing is about 500 m. Error ellipses for the 95 per cent confidence level are shown with yellow lines. Red stars correspond to the reference location, green stars to the estimated locations.

Substitution of E defined by eqs (2) or (3) into (4) shows that the source group time delay function for both types of waves can be rewritten as

$$\delta t_U = \frac{A_1 \cos(\varphi + \alpha_1) + A_3 \cos(3\varphi + \alpha_3)}{1 + A_2 \cos(2\varphi + \alpha_2) + A_4 \cos(4\varphi + \alpha_4)}, \quad (5)$$

where A_i and α_i ($i = 1, 4$) are frequency-dependent functions. Thus, the group time delay is an odd function of azimuth and in most cases the numerator will dominate the azimuthal dependence. The odd-symmetry of the dependence implies that antipolar observations (observations that differ in azimuth φ by 180°) will not cancel one another, but will actually add constructively.

In our location procedures we assume that the source mechanism is unknown even though it may have been estimated by other means. We do this because source depth typically is not well known but source group time delays for Rayleigh waves are strongly dependent on source depth in the period range we use (5–12 s). Source depth is typically more difficult to constrain than mechanism, except in unusual circumstances, and corrections of observed group time delays for source mechanism when source depth is not well known would be unreliable. Thus, source group time delays imposed by seismic events act to bias the location procedure that we present here and in Paper I. Locations will be minimally biased for events with small source group time delays. Paper I shows that Rayleigh wave source group time delays are not small for particular types of earthquakes at depths between about 2 and 5 km, for which bias may be as high as several kilometres. However, we show here that source group time delays for Love waves are much smaller than for Rayleigh waves, and this is the motivation for introducing Love waves into the location procedure.

Figs 5 and 6 aim to provide some understanding of the difference in the expected magnitude of the source group time-shift for Rayleigh and Love waves. Fig. 5 shows in a simplified version the source phase delays from eqs (2) and (3). The simplification includes setting both terms in square brackets to 1, thus removing the dependence on source-mechanism and providing a kind of average over azimuth. Clearly, the source phase shift for Rayleigh waves is significantly smaller than for Love waves for source depths between 1 and 15 km. However, the source group time-shift is related to
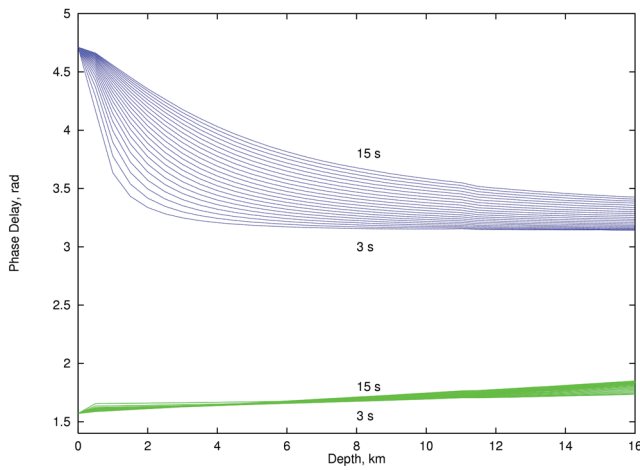
Figure 5. An average (over azimuth and source mechanism) source phase delay as a function of source depth at different periods from which the average source phase time delay can be computed. The averaging process removes the effect of the source mechanism and these results are plotted versus depth. Individual lines are for different periods ranging from 3 to 15 s, where green lines are Love waves and red lines are Rayleigh waves. The variation of this ratio with period provides an estimate of group time delay δt_U and, for each event depth shown here, the variation of the ratio is seen to be much smaller for Love than Rayleigh waves.

the frequency dependence of the source phase shift (eq. 4). Fig. 5 illustrates that the change in the source phase shift with period from 5 to 14 s period for Love waves is much smaller than for Rayleigh waves. This is also seen clearly in Fig. 6, which shows average curves of the source group time-shift δt_U as a function of period for several source depths and both types of waves. The range of δt_U values for Rayleigh waves is about 10 times greater than for Love waves.

Figs 7–9 present a compendium of theoretical calculations of the source group time delay δt_U as a function of different types of source mechanism, source depth and wave period for both Love and Rayleigh waves. These results are computed relative to a crustal model in Nevada from the global model of Shapiro & Ritzwoller (2002). Four different source mechanisms are used here and they are shown with different coloured beachballs (e.g. Fig. 7). We refer here and later in the paper to these four mechanisms as the red, green,
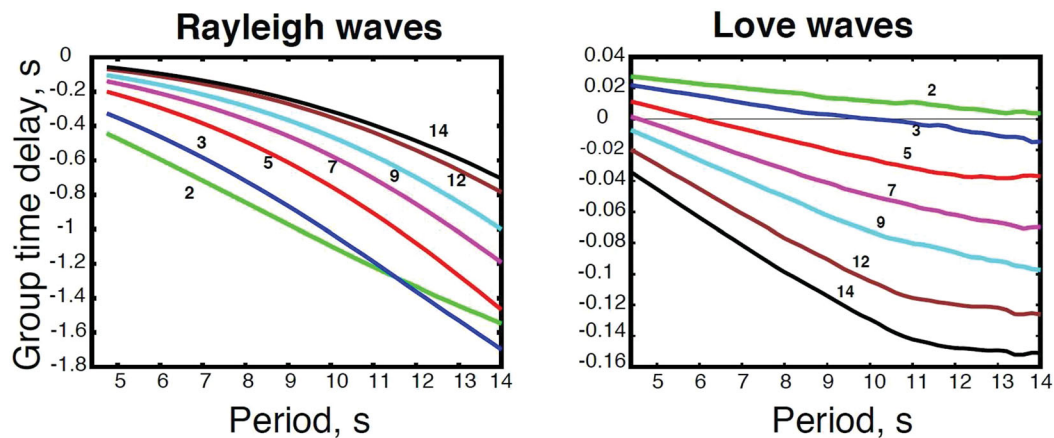
dark blue and light blue events. The results of the calculations shown in Figs 7–9 are somewhat complicated and for the sake of clarity Fig. 10 presents a blow up at 7 s period for one event type (red event in Fig. 7) at several depths. Most significantly, these figures indicate that the source group time-shifts δt_U are much smaller for Love waves than for Rayleigh waves, on average about an order of magnitude smaller. This means that epicentral locations determined using Love waves will be biased less by source mechanism. Fig. 10 also demonstrates the odd-dependence of the group time delays on azimuth.

To further clarify the method we present examples of epicentral location using simulated seismograms for a set of theoretical earthquakes with different source mechanisms and depths located in central Nevada. Fig. 11 presents the locations of the base and remote stations used in the simulation. Synthetic seismograms and Green's functions (replacing EGFs) are computed for each theoretical earthquake and the location procedure described is applied. Examples of misfit surfaces for Rayleigh and Love waves, respectively, are presented in Figs 12(a) and (b) for the red focal mechanism shown in Fig. 7 at 5 km depth. This earthquake type and depth are chosen because they provide large Rayleigh-wave group time-shifts, which results in a large epicentral bias using Rayleigh waves alone as can be seen in Fig. 12(a). In Fig. 12(a), the Rayleigh-wave location is biased by about 2.0 km. In contrast, for this event there is very low bias using Love waves alone, as Fig. 12(b) illustrates. Weighting Love waves and Rayleigh waves equally ($\lambda_R = \lambda_L = 0.5$ in eq. 1) in the location algorithm, reduces the bias appreciably, although bias does remain at about 1.0 km, as seen in Fig. 12(c). However, if we weight inversely by minimum misfit, which is very low for Love waves ($\lambda_L = 0.95$) and considerably larger for Rayleigh waves ($\lambda_R = 0.05$), then the resulting joint location is again essentially unbiased, as Fig. 12(d) shows.

We repeat this procedure systematically to estimate location bias for the four different mechanisms (red, green, light blue and dark blue) shown in Fig. 7 that occur at depths ranging from 1 to 25 km and with different data (Rayleigh, Love, joint) applied in the location procedure. Estimated bias using Rayleigh waves alone is shown in Fig. 13(a), using Love waves alone is shown in Fig. 13(b), using equally weighted Rayleigh and Love waves jointly is shown in Fig. 13(c) and using Rayleigh and Love waves jointly but weighted by misfit is shown in Fig. 13(d). Fig. 13(a) is similar to a result presented in Paper I, illustrating that location bias for Rayleigh waves
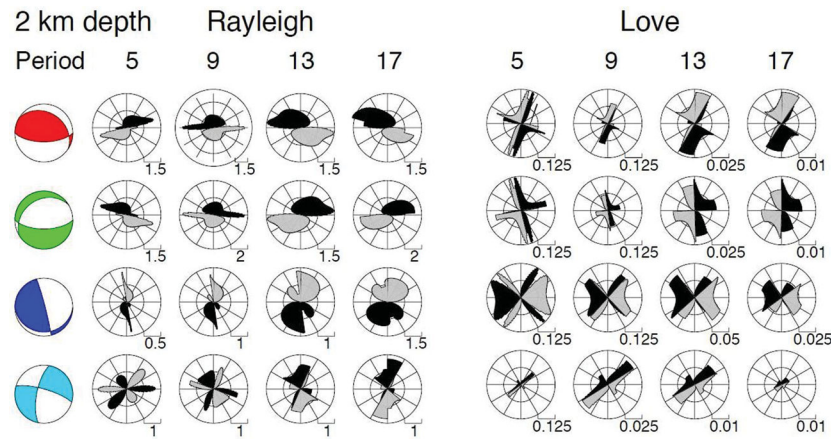

Figure 6. The average source group time delay δt_U for Rayleigh and Love waves as a function of period. Results are computed from the curves shown in Fig. 5. Numerals near the curves are the source depths in kilometres. δt_U for Love waves is shown here to be on average about 10 times smaller than for Rayleigh wave.

Figure 7. A compendium of source group time delays (in seconds) for Rayleigh and Love waves. Results are presented for four different source mechanisms shown with beachballs at left (red, green, dark blue and light blue), at four periods (5, 9, 13and 17 s), for a source depth of 2 km. Black delays are positive and grey delays are negative.
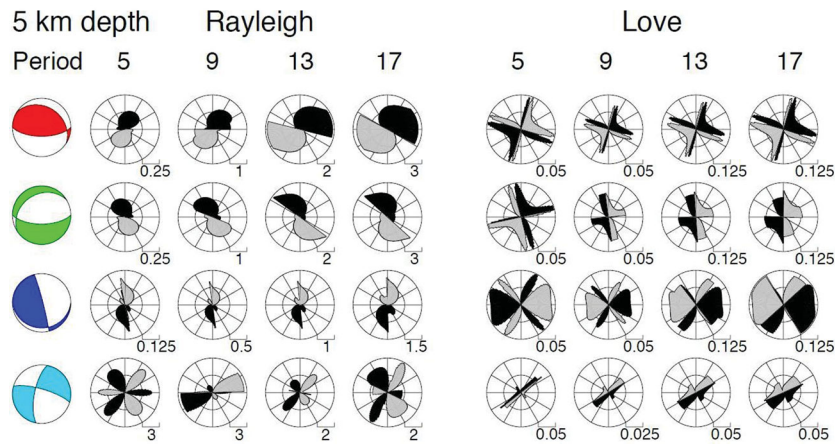

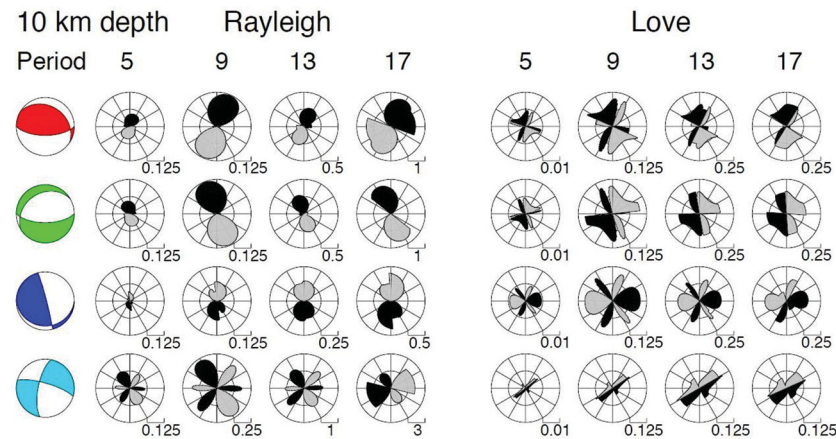**Figure 8.** Same as Fig. 7, but for a source depth of 5 km.

Figure 9. Same as Fig. 7, but for a source depth of 10 km.

can be large, up to several kilometres, for certain types of events that occur between depths of 2 and 5 km. (This figure differs slightly from the comparable figure in Paper I in which large epicentral shifts more than 3 km from the input location were not considered and Paper I, therefore, slightly underestimated the level of bias.) Fig. 13(b) illustrates that locations based on Love waves suffer a much smaller bias, with expected values less than about 400 m.

Jointly interpreting equally weighted Rayleigh and Love waves reduces the Rayleigh-wave bias substantially, but residual bias at an expected level of about 1 km would remain for events between 2 and 5 km depth as Fig. 13(c) shows. Finally, the location bias based on the joint location that differentially weights Rayleigh and Love waves inversely by misfit illustrates that the resulting bias is very low (Fig. 13d). Bias is even lower than for Love waves alone
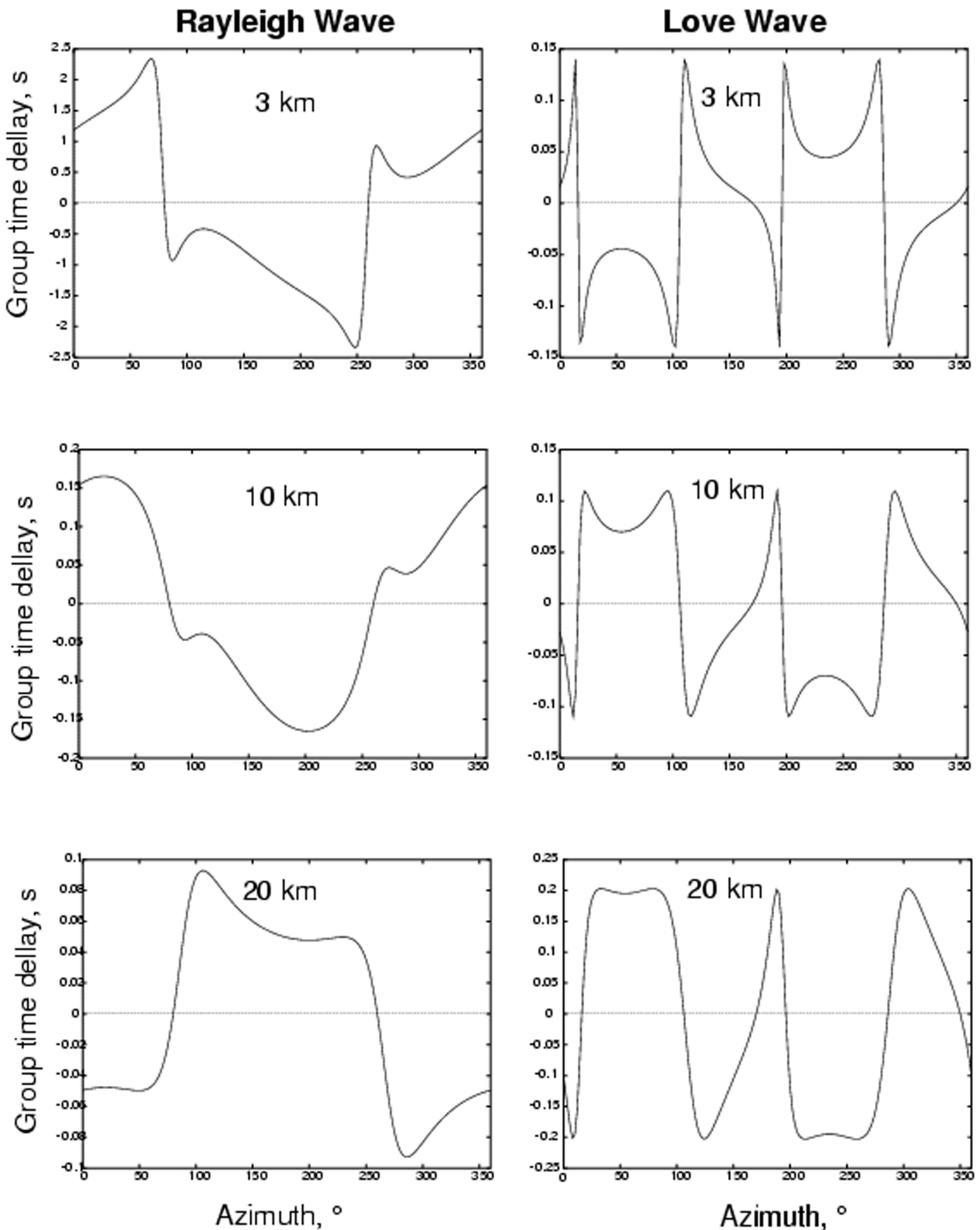
Figure 10. Theoretical group time delays δt_U at 7 s period for the source mechanism shown in red on Fig. 7 for different source depths (3, 10 and 20 km) for Rayleigh and Love waves.

because the effect of including the Rayleigh wave is to cancel part of the Love-wave bias.

It is tempting to conclude from these synthetic experiments that differentially weighting Rayleigh and Love waves based on min-

imum misfit would produce a largely unbiased estimator. This is true for noise-free data, but for real data the SNR of Love waves is typically lower than of Rayleigh waves and the minimum Love-wave misfit is not much lower than the Rayleigh-wave misfit even in
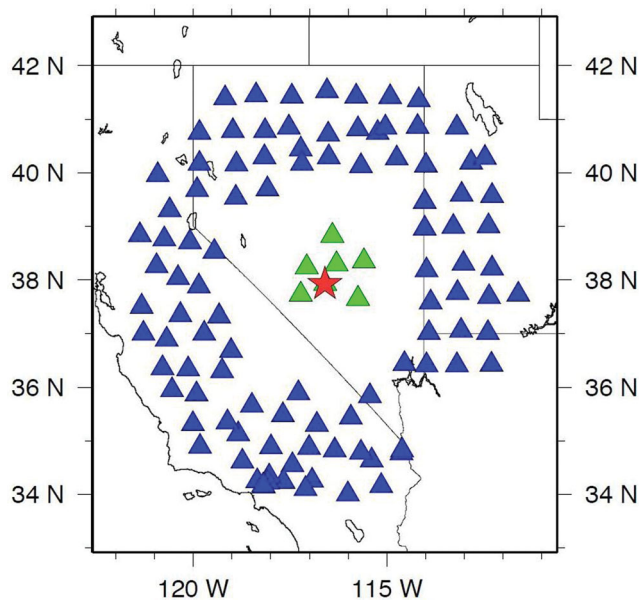
Figure 11. The network of base (green triangles) and remote (blue triangles) stations used in the synthetic location experiment. The red star is the location of the virtual source where the event is located at 5 km depth and the source mechanism is the red mechanism shown in Fig. 7.

the best cases. In fact, on average, Love-wave misfit is higher than Rayleigh-wave misfit as Figs 4(a) and (b) illustrates. In practice, it is difficult with real data to identify those events for which the Rayleigh-wave location would be biased. Although misfit is an excellent guide for synthetic data, for real data it is at best imperfect. For this reason, in presenting results with real data we will only show joint locations that weight Rayleigh and Love waves equally. A better scheme may be found for particular applications, however.

We note based on the synthetic experiments that if notable differences in locations are found by separately using Rayleigh and Love waves then the Rayleigh-wave location may be biased and it may be better for the Love-wave location to take precedence. This observation could be used as the basis for a weighting scheme, but it could also mean that the Love-wave location is unreliable. For this reason, we do not explore the method of differential weighting based on differences in epicentral locations of the wave types separately. However, such an observation could be taken as qualitative evidence that the event occurred at relatively shallow depths which is where Rayleigh-wave locations are substantially biased (between 2 and 5 km in the considered simulation). In the observational results presented in Section 5, the separate Rayleigh- and Love-wave locations are all consistent with one another, which means that the Rayleigh-wave locations for these events are probably not severely biased and the earthquakes probably did not occur between 2 and 5 km depth.

4 DATABASE OF RAYLEIGH AND LOVE EGFs AND GROUP VELOCITY CURVES FOR THE WESTERN UNITED STATES

The database for Rayleigh- and Love-wave EGFs that has been used in this study was developed at the University of Colorado for data recorded in the United States between the years 2005 and 2011 using the methodology described by Bensen *et al.* (2007) and Lin *et al.* (2008). Broad-band three-component seismograms observed at over 950 permanent and temporary stations from the TA component of

USArray were used for this purpose. This database comprises about 350 000 Rayleigh- and Love-wave interstation cross-correlation functions. For all EGFs in this database SNR was estimated and individual EGFs were retained only if SNR >10. Data processing includes the automatic two-step FTAN typically between about 5 and 12 s period. The first step in the procedure provides the raw FTAN diagram and the second step applies phase-match filtering (Herrin & Goforth 1977; Levshin & Ritzwoller 2001) to create a cleaned FTAN diagram of the fundamental Rayleigh and Love waves largely freed from interference with other waves, coda and local noise. The FTAN image is used to determine the group times in the range of periods where the power of the narrow-band output signal is not less than 95 per cent of the maximum power.

5 JOINT APPLICATION OF RAYLEIGH AND LOVE WAVES TO LOCATE REFERENCE EVENTS IN WESTERN UNITED STATES

We now present applications of the revised location method to 10 reference events that occurred in the western United States between 2005 and 2008. These include the Crandall Canyon Mine collapse in Utah on 2007 August 6 (Pechmann *et al.* 2007), which is a very shallow event whose location using Rayleigh wave EGFs was described in Paper I, two well-located events in California and Utah, the large Wells earthquake in northern Nevada, and a sequence of six aftershocks of the Wells earthquake that we refer to as aftershocks #1– #6 (Mendoza & Hartzell 2009). Source parameters for these events are listed in Table 1. Unfortunately, none of the reference events are located by the authoritative source better than about 1 km and for most events uncertainties are not well known, but 1 km is probably a reasonable 90 per cent (2σ) uncertainty estimate, on average.

The estimated epicentral locations for the 10 reference events are summarized in Table 2. Each location is compared with the reference location for Rayleigh waves alone (Ref-R), Love waves alone (Ref-L) and jointly using Rayleigh and Love waves weighted equally (Ref-RL) such that $\lambda_R = \lambda_L = 0.5$ in eq. (1). In each column, the difference in kilometres between the reference location and the estimated location is listed. In addition, the rms misfit at the estimated epicentral location is presented for all three estimators (R, L, RL). Finally, the semi-major axis of the error ellipse (95 per cent confidence) is presented for each of the estimators. For the joint location, we only present results where the Rayleigh and Love waves are weighted equally.

Other estimators could be defined that would produce somewhat different results than those we present here. In particular, as with the synthetic experiment discussed earlier, one could weight the Rayleigh and Love waves inversely by minimum misfit. However, inspection of Table 2 reveals that for the reference events the minimum misfit is approximately the same for Rayleigh and Love waves so that the result of this weighting scheme would be approximately the same as applying equal weights.

As noted earlier, the locations of the reference events are probably known to about 1 km, on average. This may be worse for the large Wells earthquake (2008 February 21), however, which has a rupture length of about 5 km (Mendoza & Hartzell 2009) and our locations may be of the centroid of this event. The difference between the estimated location and the reference location, therefore, is probably not a reliable quality criterion for locations within 1–2 km of the reference location. For these 10 events, the Rayleigh-wave locations agree quite well with the reference locations; the discrepancy being
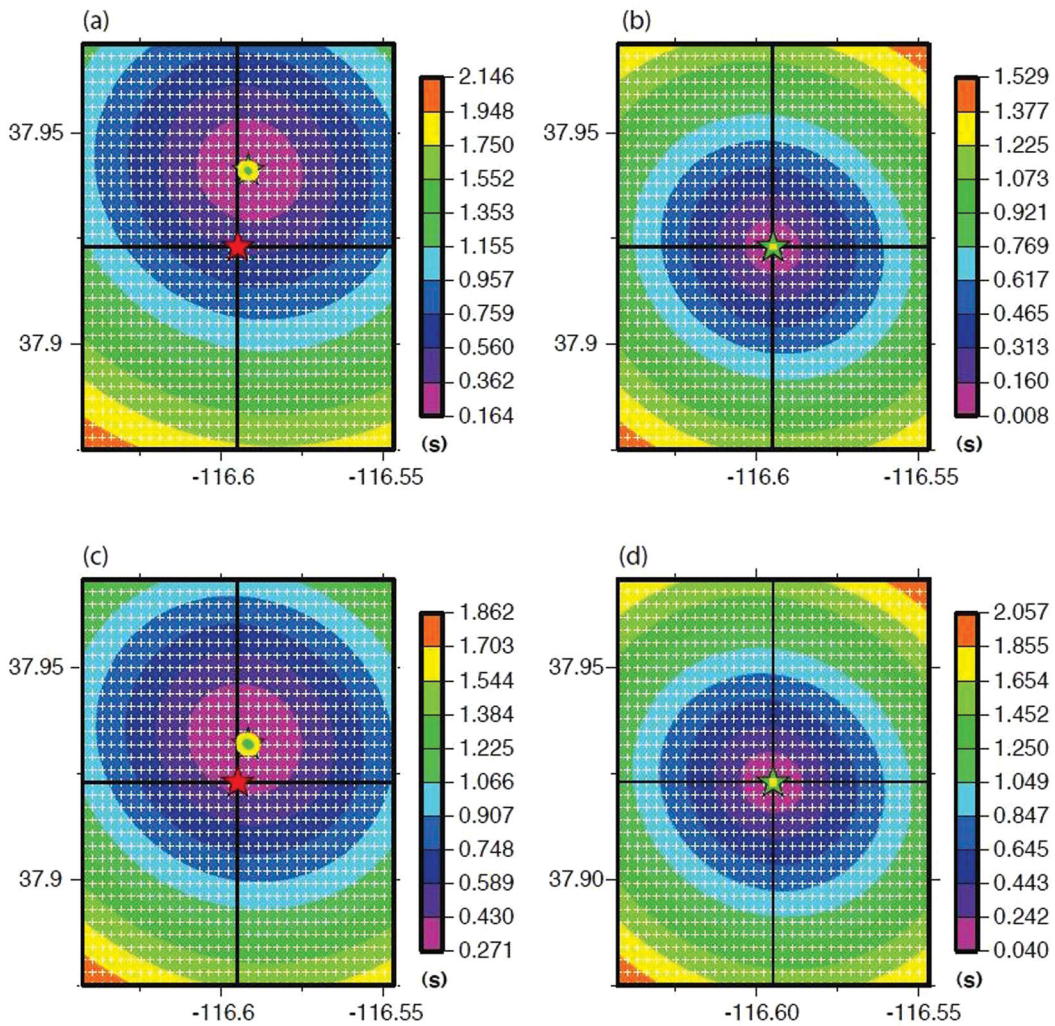
Figure 12. Simulated misfit surfaces as described in Fig. 4, but for the virtual source whose location is shown in Fig. 11 at 5 km depth and the source mechanism is the red mechanism shown in Fig. 7. Grid spacing is about 300 m.

greater than 1.0 km only for three of the events and not larger than 1.3 km for any of the events. It is, therefore, unlikely that the Rayleigh-wave location is badly biased for any of these events. This is evidence that the depths of these events are probably not between 2 and 5 km and/or the events do not have mechanisms that would cause a large bias. For this reason, we do not expect the joint inversion to provide a substantial improvement over the use of Rayleigh waves alone because the joint inversion is only expected to be appreciably better when the Rayleigh-wave location is badly biased. The choice of the 10 reference events used here is unfortunate in this regard, but identifying well-located events in the western United States that are definitely between 2 and 5 km depth is a challenging task.

The Love-wave locations alone also agree quite well with the reference locations, but the agreement is not as good as with the Rayleigh waves. Five Love-wave locations have a discrepancy relative to the reference location greater than 1.0 km with the largest discrepancy being 1.9 km. The joint location, however, does agree somewhat better with the reference locations than either the Rayleigh- or Love-wave locations alone.

Inspection of the minimum misfits (F_R, F_L, F_{RL}) in Table 2 shows that the Rayleigh-wave misfit averages about 0.9 s whereas the average Love-wave misfit is slightly higher, equalling about

1.05 s. This illustrates the point made earlier that differentially weighting Rayleigh- and Love-wave misfit in the joint location will produce little change from the equal weighting scheme. The joint location misfit is approximately the average of these values, being about 1.0 s. The level of misfit reported here results predominantly from measurement error. The data sampling rate is 1 sps (sample per second), so it is unlikely to achieve average misfit values below 0.5 s, on average. If any of the reference events were to produce badly biased locations based on Rayleigh waves, then the Rayleigh-wave misfit would have been substantially larger than 1.5 s, which we do not observe here. The largest misfit values are for the Crandall Canyon mine collapse, because surface waves are relatively weak for this event.

The 95 per cent semi-major axis of the confidence ellipses for Rayleigh waves average about 1.45 km, which is smaller than the 1.9 km average for Love waves. This results from the lower signal-to-noise level, on average, for Love waves compared with Rayleigh waves. Thus the Love-wave misfit is higher and the number of Love-wave measurements is lower. The smallest error ellipses are usually for the joint location method because the number of measurements is higher than for either Rayleigh or Love waves alone. The joint error ellipses for most of the events average about 1.5 km. The principal exception is for the California earthquake, which has much
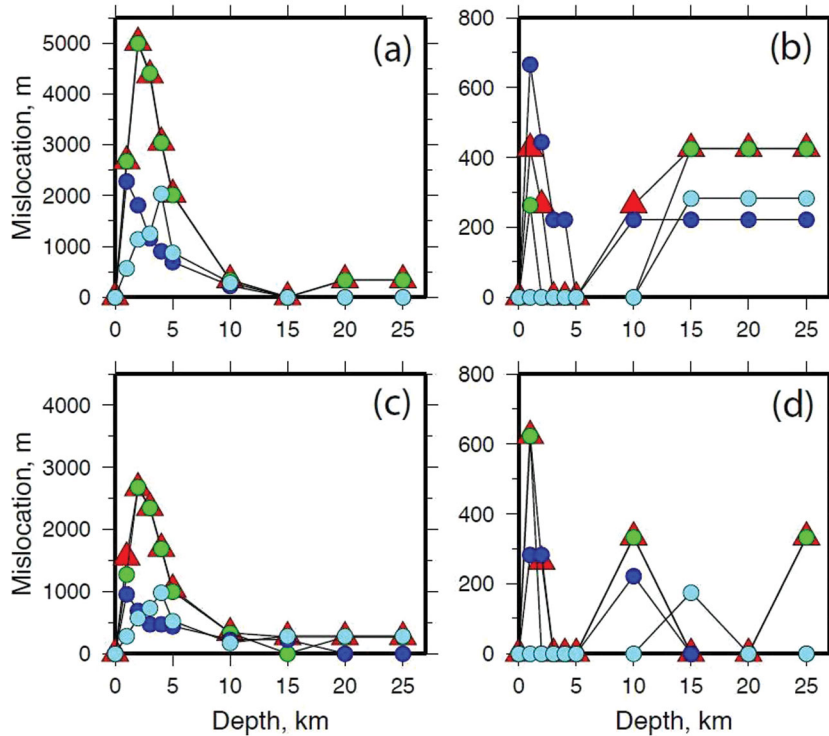
Figure 13. Summary of the mislocations found in the synthetic experiment as a function of the source depth for the four source mechanisms shown in Fig. 7: red, green, dark blue and light blue. In (a) Rayleigh waves are used alone, in (b) Love waves are used alone and in (c) Rayleigh and Love waves are used jointly and weighted identically. In (d) Rayleigh and Love waves are used jointly and weighted inversely by the minimum misfit for each wave type.

Table 2. Locations using Rayleigh (R) waves, Love waves (L) and both waves (RL).

Event	Ref-R (km)	Ref-L (km)	Ref-RL (km)	Misfit (s)			Ellipse (km)		
				R	L	RL	R	L	RL
Earthquake, CA	0.7	1.9	0.7	1.2	1.4	1.5	2.6	3.9	2.7
Mine collapse, UT	0.4	0.7	0.7	1.4	1.6	1.4	1.4	1.7	1.2
Earthquake, UT	1.3	0.0	0.4	0.9	1.3	1.3	1.7	3.1	1.7
Wells Event, NV	0.6	1.1	0.6	0.7	1.0	0.9	1.1	1.7	1.1
Aftershock#1	0.7	0.7	0.4	0.7	0.9	0.8	1.1	1.4	0.9
Aftershock#2	0.4	0.6	0.4	1.0	1.1	1.0	1.8	2.4	1.4
Aftershock#3	1.1	0.7	0.7	0.7	0.8	0.7	1.0	1.3	0.8
Aftershock#4	0.0	1.0	0.7	0.9	0.8	0.9	1.4	1.4	1.0
Aftershock#5	1.2	1.4	1.2	0.8	0.8	0.8	1.4	1.5	1.0
Aftershock#6	0.4	1.2	0.7	0.6	0.8	0.8	1.1	1.7	1.1

Notes: 'Ref-R' is the distance between the reference location and the Rayleigh-wave location. 'Ref-L' is the same but for Love waves. 'Ref-RL' is the same but using both types of waves. 'Misfit' is the minimum value (s) of the misfit functionals F_R, F_L and F_{RL}. 'Ellipse' is the length (km) of the semi-major axis of the 95 per cent confidence ellipse. Epicentral grid spacing is 500 m for earthquakes and 200 m for the Utah mine collapse.

larger error ellipses. This is because remote stations west of the earthquake did not exist (they would have to have been in the Pacific Ocean) and few remote stations yet existed in the USArray TA east of the earthquake at this time (2005 April), so the number of stations is much lower for this event that for the other events. The Utah earthquake suffers a somewhat similar problem, as the TA was truncated to the east and northeast of the earthquake when it occurred (2007 August), which reduced the number of available stations.

Error ellipses will accurately represent the quality of the location only when the location estimates are unbiased. Because evidence shows that for the events considered here the Rayleigh waves do not yield badly biased location estimates, comparison between error ellipses is a reliable means to judge the solutions. We see that for eight of the 10 events, the joint location has a smaller error ellipse than either the Rayleigh- or the Love-wave location. This is not surprising because the size of the error ellipse scales inversely with the number of measurements. In terms of the totality of evidence we present here we believe that the reduction in the size of the error ellipses is probably the best determinant of the improved quality of the joint location estimator.

The estimated error ellipses are shown in Figs 14 and 15. Two principal observations are worthy of note. (1) The Rayleigh- (red ellipses) and Love- (blue ellipses) wave error ellipses overlap and, therefore, their locations are consistent with one another. In fact, the Love-wave error ellipse usually largely encompasses the Rayleigh-wave ellipse. This consistency results from the fact that for these events the Rayleigh-wave estimator is not badly biased. (2) The
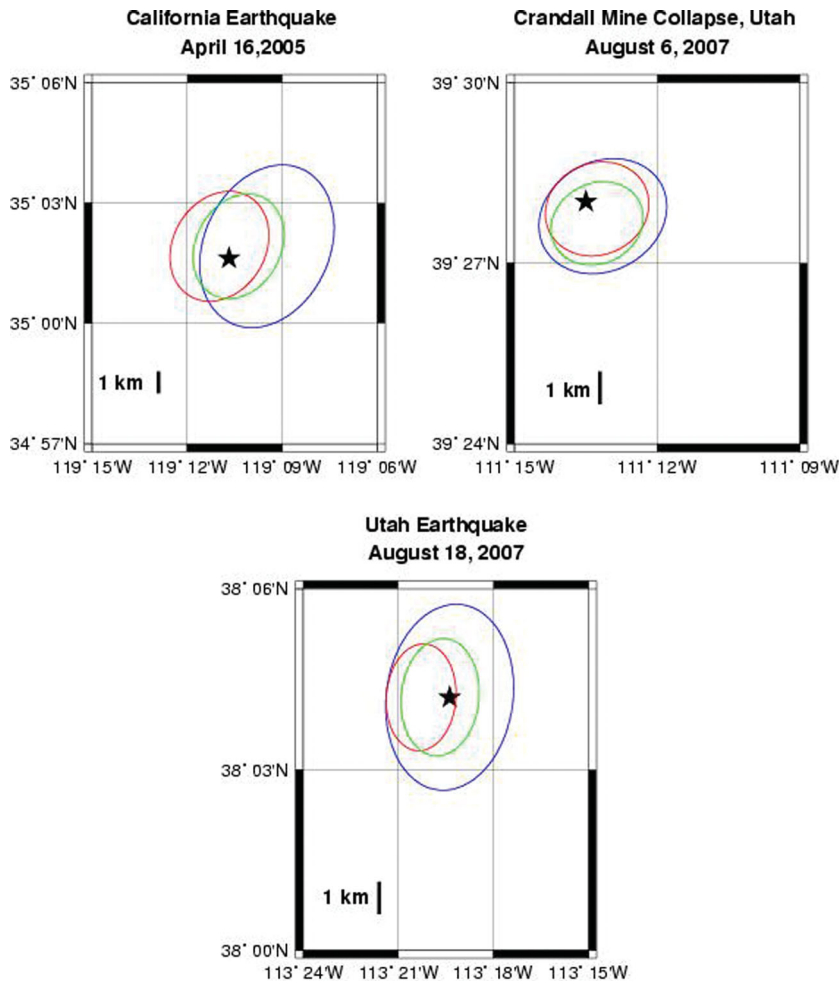
Figure 14. Locations of reference events (stars, Table 1) in California and Utah compared with locations from the methods described herein. Ellipses correspond to the 95 per cent confidence level where the location results from the Rayleigh estimator (red ellipse), the Love estimator (blue ellipse) and the joint estimator where Rayleigh and Love waves are equally weighted (green ellipse).

joint location error ellipse (green ellipses) is typically the smallest of the three ellipses and strikes a balance between the Rayleigh- and Love-wave estimates.

Finally, the absolute values of differences between the reference origin times and the origin times we estimate vary between 0.1 and 1.5 s.

6 CONCLUSIONS

Paper I (Barmin *et al.* 2011) presented a new method to estimate epicentral locations based on exploiting Rayleigh-wave EGFs obtained from ambient noise. This location procedure considers a set of hypothetical epicentral locations and one is chosen that brings the FTAN diagrams from the event observed on remote stations into optimal agreement with the FTAN diagrams for the EGFs that are observed from stations near the event to the same remote stations. Technically, this comparison is performed by cross-correlation in time between the FTAN diagrams (Levshin *et al.* 1989; Bensen *et al.* 2007). FTAN diagrams form a rather unstable basis for this method if it is to be applied systematically. In addition, Paper I showed that the estimator can be significantly biased for certain types of earthquakes in the depth range from 2 to 5 km. This paper presents a more stable algorithm based on comparing the measured group velocity curves on the event and EGF records and extends the method

to include Love waves, which we show to be much less liable to yield-biased locations than are Rayleigh waves. Love waves, however, typically are lower SNR observations than Rayleigh waves, and epicentral locations based on Love waves display higher variance than those based on Rayleigh waves. We present evidence that the epicentral locations, the result for shallow crustal events based on jointly interpreting Rayleigh and Love waves, are preferable to locations based on Rayleigh or Love waves alone. This is because the joint estimator balances the need for low bias and low variance in the location estimate.

The joint estimator is not uniquely defined. The individual contributions of the Rayleigh and Love waves may be weighted in a large number of reasonable ways. What is desired is to identify when the Rayleigh-wave location estimate is biased and to strongly weight Love-wave information in these cases. This is not trivial, however. We show here that misfit between the event records and the EGFs works well in identifying when the Rayleigh-wave estimator is biased in the low noise limit, but in real world applications to small seismic events measurement errors are large enough to render misfit to be an ineffective basis for differential weighting of Rayleigh and Love waves in the joint estimator. In the applications considered here, differentially weighting Rayleigh and Love waves by misfit would produce results similar to weighting the two wave types identically. Other ideas that may be worthy of future
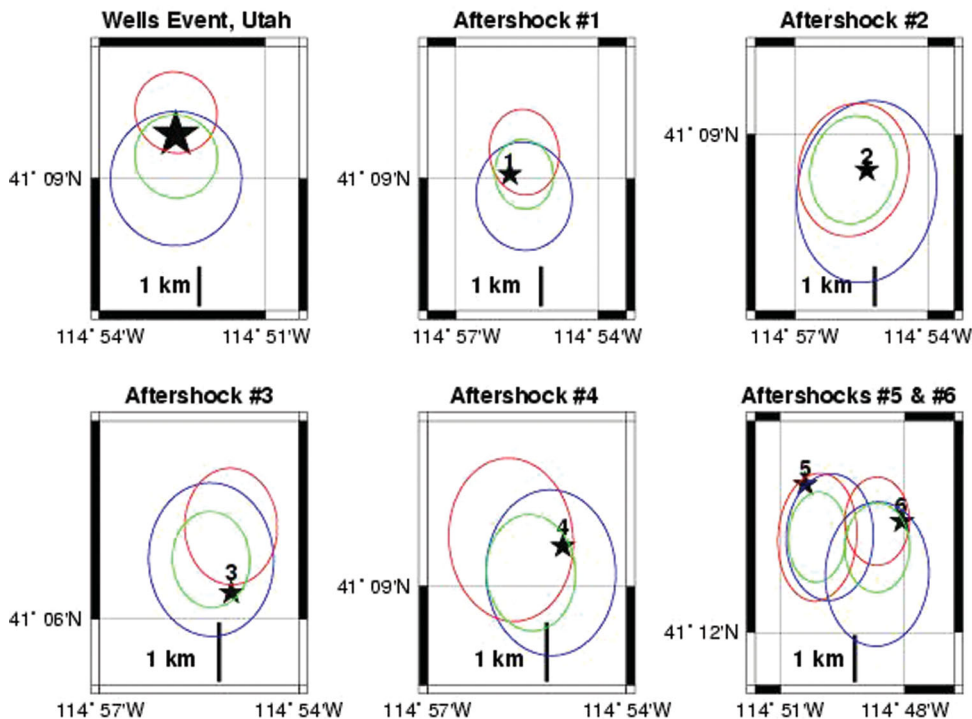
Figure 15. Same as Fig. 14, but for the location of the large Wells earthquake on 2008 February 21 and its six aftershocks (Table 1).

consideration include differentially weighting by average SNR of the event and/or EGF records, by discrepancy from a prior location estimate, or by other metrics of group velocity measurement quality. Here, we present real world applications based exclusively on weighting Rayleigh and Love wave equally in the location procedure. It is for the joint estimator defined in this way that we show that the epicentral locations of shallow crustal events are preferable to locations based on Rayleigh or Love waves alone.

The procedure presented here may also be performed by comparing theoretical group velocity curves (computed, e.g. from existing group velocity maps or a 3-D model) with the group velocity measurements obtained from the event records. We believe that the current method is preferable because it compares measurements (obtained on EGFs) with measurements (obtained on event records). However, using curves from existing group (or phase) velocity maps computed from ambient noise tomography (e.g. Shapiro *et al.* 2005; Moschetti *et al.* 2007; Yang *et al.* 2007; Lin *et al.* 2008; and many others) or from curves predicted from a 3-D model that originated by inverting ambient noise dispersion maps (e.g. Yang *et al.* 2008; Moschetti *et al.* 2010a,b; Zheng *et al.* 2011; Yang *et al.* 2012; Zhou *et al.* 2012; and others) would make the algorithm more flexible and would open the possibility to estimate other source parameters such as hypocentral depth and the moment tensor.

ACKNOWLEDGMENTS

REFERENCES

Aki, K. & Richards, P.G., 1980. *Quantitative Seismology: Theory and Methods, I,* W. H. Freeman and Co., San Francisco, CA.

Barmin, M.P., Levshin, A.L., Yang, Y. & Ritzwoller, M.H., 2011. Epicentral location based on Rayleigh wave empirical Green's functions from ambient seismic noise, *Geophys. J. Int.,* **184,** 869–884, doi:10.1111/j.1365-246X.2010.04879.x.

Bensen, G.D., Ritzwoller, M.H., Barmin, M.P., Levshin, A.L., Lin, F., Moschetti, M.P., Shapiro, N.M. & Yang, Y., 2007. Processing seismic ambient noise data to obtain reliable broad-band surface wave dispersion measurements, *Geophys. J. Int.,* **169**(3), 1239–1260, doi:10.1111/j.1365-246X.2007.03374.x.

Flinn, E.A., 1965. Confidence regions and error determinations for seismic event locations, *Rev. Geophys.,* **3,** 157–185.

Herrin, E. & Goforth, T., 1977. Phase-matched filtering: application to the study of Rayleigh waves, *Bull. seism. Soc. Am.,* **67,** 1259–1275.

Herrmann, R.B., Benz, H. & Ammon, C.J., 2011. Monitoring the earthquake process in North America, *Bull. seism. Soc. Am.,* **101**(N6), 2609–2625, doi:10.1785/0120110095.

Jordan, T.H. & Swerdrup, K.A., 1981. Teleseismic location techniques and their application to earthquake clusters in the South-Central Pacific, *Bull. seism. Soc. Am.,* **71**(4), 1105–1130.

Levshin, A.L. & Ritzwoller, M.H., 2001. Automatic detection, extraction, and measurement of regional surface waves, *Pure appl. Geophys.,* **158,** 1531–1545.

Levshin, A.L., Pisarenko, V.F. & Pogrebinsky, G.A., 1972. On a frequency-time analysis of oscillations, *Ann. Geophys.,* **28,** 211–218.

Levshin, A.L., Yanovskaya, T.B., Lander, A.V., Bukchin, B.G., Barmin, M.P., Ratnikova, L.I. & Its, E.N., 1989. *Seismic Surface Waves in Laterally*

Inhomogeneous Earth, ed. Keilis-Borok, V.I., Kluwer Academic Publishers, Dordrecht.

Levshin, A.L., Ritzwoller, M.H. & Resovsky, J.S., 1999. Source effects on surface wave group travel times and group velocity maps, *Phys. Earth planet. Inter.,* **115,** 293–312.

Lin, F., Moschetti, M.P. & Ritzwoller, M.H., 2008. Surface wave tomography of the western United States from ambient seismic noise: Rayleigh and Love wave phase velocity maps, *Geophys. J. Int.,* **173**(1), 281–298, doi:10.1111/j1365-246X.2008.03720.x.

Mendoza, C. & Hartzell, S., 2009. Source analysis using regional empirical Green's functions: the 2008 Wells, Nevada, earthquake, *Geophys. Res. Lett.,* **36,** L11302, doi:10.1029/2009GL038073.

Moschetti, M.P., Ritzwoller, M.H. & Shapiro, N.M., 2007. Surface wave tomography of the western United States from ambient seismic noise: Rayleigh wave group velocity maps, *Geochem. Geophys. Geosyst.,* **8,** Q08010, doi:10.1029/2007GC001655.

Moschetti, M.P., Ritzwoller, M.H. & Lin, F.C., 2010a. Seismic evidence for widespread crustal deformation caused by extension in the western USA, *Nature,* **464**(7290), 885–889.

Moschetti, M.P., Ritzwoller, M.H., Lin, F.C. & Yang, Y., 2010b. Crustal shear velocity structure of the western US inferred from amient noise and earthquake data, *J. geophys. Res.,* **115,** B10306, doi:10.1029/2010JB007448.

Pechmann, J.C., Arabasz, W.J., Pankow, K.L., Burlacu, R. & McCarter, M.K., 2007. Seismological report on the 6 Aug 2007 Crandall Canyon Mine Collapse in Utah, *Seismol. Res. Lett.,* **79**(5), 620–636.

Shapiro, N.M. & Ritzwoller, M.H., 2002. Monte-Carlo inversion for a global shear velocity model of the crust and upper mantle, *Geophys. J. Int.,* **151,** 88–105.

Shapiro, N.M., Campillo, M., Stehly, L. & Ritzwoller, M.H., 2005. High resolution surface wave tomography from ambient seismic noise, *Science,* **307**(5715), 1615–1618.

Yang, Y., Ritzwoller, M.H., Levshin, A.L. & Shapiro, N.M., 2007. Ambient noise Rayleigh wave tomography across Europe, *Geophys. J. Int.,* **168**(1), 259.

Yang, Y., Ritzwoller, M.H., Lin, F.-C., Moschetti, M.P. & Shapiro, N.M., 2008. The structure of the crust and uppermost mantle beneath the western US revealed by ambient noise and earthquake tomography, *J. geophys. Res.,* **113,** B12310, doi:10.1029/2008JB005833.

Yang, Y., Ritzwoller, M.H., Zheng, Y., Shen, W., Levshin, A.L. & Xie, Z., 2012. A synoptic view of the distribution and connectivity of the mid-crustal low velocity zone beneath Tibet, *J. geophys. Res.,* **117,** B04303, doi:10.1029/2011JB008810.

Zheng, Y., Shen, W., Zhou, L., Yang, Y., Xie, Z. & Ritzwoller, M.H., 2011. Crust and uppermost mantle beneath the North China Craton, northeastern China, and the Sea of Japan from ambient noise tomography, *J. geophys. Res.,* **116,** B12312, doi:10.1029/2011JB008637.

Zhou, L., Xie, J., Shen, W., Zheng, Y., Yang, Y.. Shi, H. & Ritzwoller, M.H., 2012. The structure of the crust and uppermost mantle beneath South China from ambient noise and earthquake tomography, *Geophys. J. Int.,* **189,** 1565–1583, doi:10.1111/j.1365-246X.2012.05423.x.